Structural and Electronic Factors That Influence Oxygen Affinities: A Spectroscopic Comparison of Ferrous and Cobaltous Oxymyoglobin†

Lisa M. Miller and Mark R. Chance*

Department of Physiology and Biophysics, Albert Einstein College of Medicine of Yeshiva University, Bronx, New York 10461

Received February 27, 1995; Revised Manuscript Received May 26, 1995®

ABSTRACT: Various structural and electronic factors that result in similar rates of oxygen association (k_{on}) and differing rates of oxygen dissociation (k_{off}) for ferrous (FeMb) and cobaltous (CoMb) myoglobin have been investigated. Similar values for k_{on} indicate similar barriers to oxygen binding for CoMb and FeMb. Through optical spectroscopy, we have found that the stable quantum yields of photolysis for $CoMbO_2$ (0.55 ± 0.05) and $FeMbO_2$ (0.50 ± 0.05) at 10 K are the same. The X-ray absorption near edge spectra (XANES) of CoMb and FeMb reveal similar metal−heme displacements for the deoxy, oxy, and low temperature photoproduct states of CoMb and FeMb. Thus, similar barriers to ligand binding, indicated by similar k_{on}'s and photoproduct yields for CoMb and FeMb, correlate with the metal−heme displacements for the oxy, deoxy, and low temperature photoproduct states of CoMb and FeMb. Lower values of k_{off} for $FeMbO_2$ versus $CoMbO_2$ imply different barriers to oxygen release for the two species. X-ray edge positions of CoMb and FeMb indicate a substantial transfer of electron density from the metal to the ligand upon oxygenation. The distribution of electron density throughout the M−O−O moiety differs for $CoMbO_2$ and $FeMbO_2$. Resonance Raman spectroscopy has demonstrated that the Co−O bond is weaker when compared to Fe−O [Tsubaki, M., & Yu, N. T. (1981) *Proc. Natl. Acad. Sci., U.S.A. 78,* 3581]. We have used photolyzed/unphotolyzed Fourier Transform Infrared (FTIR) difference spectra of $CoMb^{16}O_2$, $CoMb^{18}O_2$, $FeMb^{16}O_2$, and $FeMb^{18}O_2$ to show that the dioxygen stretching frequency, ν(O−O), in $CoMbO_2$ (~1138 cm^{-1}) is higher than $FeMbO_2$ (~1131 cm^{-1}). The dioxygen stretching frequency in $CoMbO_2$ is closer to that of heme protein models lacking a hydrogen bond to the distal histidine, suggesting that formation of the hydrogen bond in $FeMbO_2$ provides a greater effect on the distribution of electron density throughout the Fe−O−O••HN moiety, potentially stabilizing a more ionic Fe−O−O bond. These findings demonstrate important electrostatic differences in the distal environments of $CoMbO_2$ and $FeMbO_2$, resulting in different barriers to oxygen release.

Characterization of the ligand-bound and photoproduct states of myoglobin, hemoglobin, and other hemeproteins is essential to understanding the mechanisms of ligand-binding and photolysis. Elucidating the functional role of the heme iron in these processes is crucial. An excellent means of doing so is by studying metal-substituted hemeproteins. The iron center in hemoglobin and myoglobin has been replaced by cobalt (Hoffman & Petering, 1970), copper (Fabry et al., 1968), manganese (Fabry et al., 1968; Yonetani et al., 1970), and nickel (O'Hagen, 1961), but only cobalt-substituted myoglobin and hemoglobin have been shown to reversibly bind oxygen (Hoffman & Petering, 1970). The oxygen affinity for cobalt myoglobin (CoMb) is lower than for native ferrous myoglobin (FeMb), resulting from a rate of oxygen dissociation (k_{off}) that is much higher for $CoMbO_2$. The rate of oxygen association (k_{on}) for CoMb is comparable to that of FeMb (Table 1) (Antonini & Brunori, 1971; Yamamoto et al., 1974). Therefore, an investigation of the structural and electronic factors that result in similar physiological rates of oxygen binding and unique rates of oxygen release for CoMb and FeMb provides valuable information on the role of iron in these processes.

The physiological rate of oxygen association in myoglobin (k_{on}) reflects the overall barrier to oxygen binding. This barrier involves (1) diffusion of the ligand through the protein matrix, i.e., the *outer barrier*, and (2) reaction of the ligand with the heme iron, i.e., the *inner barrier* (Carver et al., 1990; Quillin et al., 1995). Flash photolysis and recombination studies of NO, O_2, and CO with myoglobin at room temperature indicate that these three gaseous ligands diffuse through the protein at similar speeds and that the major differences in the physiological rates of ligand association to myoglobin are a result of distinct barriers at the heme (Doster et al., 1982; Carver et al., 1990; Gibson et al., 1992; Quillin et al., 1995). In other words, the outer barrier for these ligands is similar, and the variations in k_{on} for MbCO, MbO_2, and MbNO come from different inner barriers to ligand binding. Carver, et. al. (1990) have suggested that the heights of the inner and outer barriers are approximately equal for O_2 binding at neutral pH. This result is in contrast to CO binding, in which the inner barrier is noticeably higher.

Early work by Frauenfelder and co-workers (Austin et al., 1975) has shown that the inner (also called *geminate*) rebinding barrier can be isolated by flash photolysis of the ligand at cryogenic temperatures, where the protein matrix is frozen and the ligand is unable to escape from the distal pocket. Chance et al. (1990) have proposed a direct relationship between the barrier to ligand binding and the low

† This research is supported by the NIH Grant HL-45892 (M.R.C.).
* Author to whom correspondence should be addressed. Phone: (718) 430-4136. Internet: mrc@aecom.yu.edu.
® Abstract published in *Advance ACS Abstracts,* July 15, 1995.

0006-2960/95/0434-10170$09.00/0

Table 1: Comparison of Rate Constants and Vibrational Frequencies for Various Ferrous and Cobaltous Myoglobins and Model Compounds

	k_{on} (μM^{-1} s^{-1})	k_{off} (s^{-1})	ν(M−O) (cm^{-1})	M−O (Å)	ν(O−O) (cm^{-1})
$FeMbO_2$	20[a]	10[a]	570[b]	1.83(6)[c]	1131
$CoMbO_2$	40[d]	2800[d]	540[b]	1.89(8)[e]	1138
$Mb(H64G)O_2$	140[f]	1600[f]			
$Mb(H64Q)O_2$	24[f]	130[f]			
$Fe(O_2)(T_{piv}PP)(2MeIm)$			561[g]	1.898(7)[g]	
$Fe(O_2)(T_{piv}PP)(1MeIm)$	0.49 ($P_{0.5}$)[h]		572[h]	1.75(2)[g]	1159[i]
$Co(O_2)(T_{piv}PP)(1MeIm)$	61 ($P_{0.5}$)[h]				1150[i]
$Co(O_2)Az_{piv}\alpha\alpha$			520[j]		1149[j]

[a] Antonini and Brunori (1971). [b] Tsubaki and Yu (1981). [c] Phillips (1980). [d] Yamamoto et al. (1974). [e] Petsko et al. (1978). [f] Rohlfs et al. (1990). [g] Walters et al. (1980). [h] Collman et al. (1978). [i] Collman et al. (1976). [j] Proniewicz et al. (1989).

temperature quantum yield of photolysis, where the quantum yield of photolysis (or photoproduct yield) is defined as the fraction of liganded material that is converted to "deoxy-like" photoproduct upon photolysis at cryogenic temperatures. For ligands such as O_2 and CO, where the outer barriers are approximately equal (Carver et al., 1990; Quillin et al., 1995), slower values for k_{on} imply higher inner barriers to ligand binding, which are reflected in higher observable photoproduct yields at low temperature. This trend is observed when comparing the values of k_{on} for MbCO and MbO_2 to the quantum yields of photolysis for MbCO and MbO_2; the rate of O_2 association to myoglobin is ~30 times larger than CO (Brunori et al., 1969), and the observed yield of MbO_2 photolysis has been established through optical spectroscopy to be 0.4 ± 0.1 at 8 K whereas that of MbCO is 1.0 (Chance et al., 1990). The "unphotolyzable" population in MbO_2 is representative of conformational substates that have essentially zero barrier to recombination (Ahmed et al., 1991; Chance et al., 1990; Petrich et al., 1988).

Structurally, proximal influences, such as the tilt of the proximal histidine and metal−heme displacement (M−Ct) of the deoxy and/or ligand-bound species may affect the magnitude and distributed nature of the ligand rebinding barrier (Friedman et al., 1982, 1985; Scott et al., 1985; Chance et al., 1990). For example, ligands such as CO, which rebind to a planar heme (Kuriyan et al., 1986), would be expected to have higher barriers than ligands such as O_2, which may recombine more easily to a nonplanar heme (Phillips, 1980). The prior observation of similar barriers to O_2 and CO binding in myoglobin (Doster et al., 1982) specifically failed to address the different quantum yields noted above. Those kinetic studies only probed the rates assignable to long-lived (i.e., postnanosecond) states. The entire distribution includes the "unphotolyzable" fraction that can only be observed through spectral analysis, as mentioned above.

X-ray crystallography has been used to identify the metal−heme displacements for deoxy-Mb (Phillips, 1981; Quillin et al., 1993; Schlichting et al., 1994), MbCO (Kuriyan et al., 1986; Quillin et al., 1993; Schlichting et al., 1994), MbO_2 (Phillips, 1980), and the MbCO photoproduct (Schlichting et al., 1994). The fine structure in X-ray absorption near edge spectra (XANES) has also been correlated to the iron out-of-plane distance in ferryl, ferric, and ferrous hemeproteins by calibration of spectral changes to known crystallographic data (Bianconi et al., 1984; B. Chance et al., 1984; M. Chance et al., 1986; Chance, 1986; Shiro et al., 1991). However, XANES is better suited than crystallography for determining metal−heme displacements of photolysis intermediates in which the quantum yield is less than unity since the difference techniques necessary are straightforward. Thus, a direct comparison of the metal−heme displacements for the deoxy, oxy, and low-temperature photoproducts of CoMb and FeMb can be made by examining the XANES spectra of those species, and conclusions can be drawn about the proximal barriers to oxygen binding in CoMb versus FeMb.

Oxygen binding and release are strongly influenced by distal pocket effects, i.e., the structural and electronic changes that occur in the M−O−O moiety itself and its interaction with the distal pocket residues upon oxygenation. EPR (Hoffman & Petering, 1970; Chien & Dickinson, 1972; Yonetani et al., 1974a) and Mossbauer (Spartalian et al., 1976) studies of the deoxy and oxy forms of CoMb and FeMb, respectively, reveal that there is a significant transfer of the unpaired electron density from the metal to the oxygen ligand upon oxygenation. X-ray absorption spectroscopy provides a method for directly comparing this electron density transfer in the cobaltous and ferrous species. Numerous studies have correlated the position of the X-ray edge to the effective charge on the central metal (Belli et al., 1980; Wong et al., 1984; Wirt et al., 1991; Scheuring et al., 1994). Shifts in the X-ray edge position as a ligand binds imply a reorganization of electron density between the metal and the ligand, acting as a probe of electron density redistribution after oxygen binding in myoglobin.

The distribution of electron density throughout the M−O−O moiety, including the strengths of the metal−oxygen and dioxygen bonds, polarity of the M−O−O unit, distal pocket polarity, and hydrogen bond strength, contributes to the distal barrier to oxygen binding and release in myoglobin. Resonance Raman (RR) studies have established that ν(Co−O) is weaker than ν(Fe−O), contributing to a higher value of k_{off} for $CoMbO_2$ compared to $FeMbO_2$ (Tsubaki & Yu, 1981). The dioxygen stretching frequency, ν(O−O), has been probed for $CoMbO_2$ through RR spectroscopy. However, similar RR studies have not been possible for $FeMbO_2$ due to lack of resonance enhancement of ν(O−O) (Tsubaki & Yu, 1981). Infrared spectroscopy has been used to address ν(O−O) in $FeMbO_2$, but there has been only a single report of a direct comparison of ν(O−O) for $CoMbO_2$ and $FeMbO_2$ (Maxwell & Caughey, 1974). Several modes sensitive to $FeMbO_2$ dioxygen isotopic substitution have been identified through infrared difference spectroscopy (Potter et al., 1987). More recently, the photolyzability of $FeMb^{16}O_2$ has been shown to provide an excellent means for generating difference spectra (photolyzed/unphotolyzed) at 10 K (Miller & Chance, 1994). We extend this approach to $CoMb^{16}O_2$, $CoMb^{18}O_2$, and $FeMb^{18}O_2$, providing a direct comparison of ν(O−O) for $CoMbO_2$ and $FeMbO_2$.

The polarity of the M−O−O moiety and the distal residue affects the oxygen binding kinetics in myoglobin (Carver et al., 1990; Ikeda-Saito et al., 1991; Rohlfs et al., 1990). Rohlfs, et. al. (1990) have proposed that oxygen affinity is controlled by the ability of the distal residue to stabilize a polar M−O−O unit, most notably by forming a hydrogen bond to the bound dioxygen. Comparison of the dioxygen stretches of $CoMbO_2$ and $FeMbO_2$ to models lacking the hydrogen bond to the distal histidine provides some insight into the extent of electron redistribution through the M−O−O···HN−His moiety and, thus, the polarity of the M−O−O bond.

In summary, in this paper we address the crucial role of iron in the process of oxygen-binding to myoglobin by comparing the deoxy, oxy, and low temperature photoproducts of FeMb to CoMb. We have studied the similarities in rates of oxygen association (k_{on}) and differences in oxygen dissociation (k_{off}) in $CoMbO_2$ and $FeMbO_2$ by examining factors affecting both the proximal and distal barriers to ligand binding. Low temperature quantum yields of photolysis for $CoMbO_2$ and $FeMbO_2$ are a means of probing the relative barriers to oxygen binding. We have investigated the relationship between the degree of metal−heme displacement and the proximal barrier to ligand recombination by XANES analysis of the deoxy, oxy, and low-temperature photoproduct states of cobaltous myoglobin. Distal effects involving the electronic configuration of the M−O−O moiety and its interactions with the distal pocket, which may affect the overall barrier to oxygen binding and release, have been addressed by analyzing the X-ray edge positions of deoxy- and oxy-FeMb and CoMb and by comparing the bound dioxygen stretching frequencies, ν(O−O), of $CoMbO_2$ and $FeMbO_2$.

MATERIAL AND METHODS

Horse skeletal muscle myoglobin, deuterium oxide (99.9%), glycerol, and trizma base were purchased from Sigma Chemical Co. Sodium dithionite and hydrochloric acid (36.5−38%) were purchased from J. T. Baker & Company. N_2 (99 atom %), O_2 (99 atom %), and liquid He were purchased from MG Industries. All chemicals and gases were used without further purification. Cobaltous oxymyoglobin ($CoMbO_2$) was a gift from Dr. H. C. Lee of Albert Einstein College of Medicine and was prepared from horse skeletal muscle myoglobin as described previously (Yonetani et al., 1974b). MbO_2 samples were prepared in 100 mM buffer (pD 7.0 Tris buffer in D_2O for FTIR experiments; pH 7.0 Tris buffer in 75:25 glycerol/H_2O for X-ray and optical absorption experiments) as described previously (Miller & Chance, 1994).

FTIR Spectra. Samples were placed between two CaF_2 windows using a 0.025 mm Teflon spacer and mounted in a low-temperature cryostat (Janis ST-4B) which was interfaced to a Lakeshore Temperature Controller (Model 805). Samples were cooled via a liquid helium transfer line. Spectra were taken using a Mattson Galaxy Series 5000 FTIR equipped with a liquid nitrogen-cooled MCT detector interfaced to a Gateway 386 computer. For each spectrum, 128 scans were taken at a 2 cm^{-1} resolution. Spectra of the ligand-bound sample were taken at 70, 50, 30, and 10 K as the sample was cooled. The sample was photolyzed at 10 K for 10 min per side using a high-intensity white light source (CUDA Products, Inc., Model I-150). The photolysis source was turned off and spectra of the photoproduct were taken at 10, 30, 50, 70 K as the sample was warmed. Spectral interferograms were collected and fourier transformed using FIRST software provided by Mattson, Inc. Difference spectra were generated by dividing the photoproduct spectra by the ligand-bound spectra at each respective temperature (i.e., photoproduct at 10 K/ligand-bound at 10 K) and converting from transmittance to absorbance units. Then the difference spectra were fit to a cubic polynomial baseline.

Optical Absorption Spectra. Samples were mounted and cooled as described in the previous section (*FTIR Spectra*). For these experiments, the teflon spacer thickness was 0.050 mm, and samples were on the order of 1 mM in concentration, giving an optical density in the Soret region between 0.8 and 0.9 OD. Spectra were taken using a Hewlett Packard Diode Array Spectrometer (Model HP8452A). Data collection time was 0.1 s for each spectrum to prevent photolysis of the sample by the spectrometer's deuterium source lamp. The sample was cooled to 8 K, and a spectrum of the ligand-bound oxymyoglobin (MbO_2) was taken (Figure 1). Then, the sample was photolyzed for 5 min per side using a high-intensity white light source (CUDA Products, Inc. Model I-150) or by a 2-min exposure to the spectrometer's deuterium lamp. Both photolysis sources yielded the same results and longer exposure times did not increase the degree of photolysis. The photolysis protocol was first tested with an MbCO sample, which is fully photolyzable (Chance et al., 1990). We were able to achieve 100% photolysis of the MbCO with a 2 min per side illumination by the white-light source or a 40 s exposure to the spectrometer source lamp. After photolysis, the light source was turned off and spectra of the photolyzed sample (Mb^*O_2) were taken at 10 K increments as the sample was warmed, until it had fully recombined.

First, the spectra were fit to a cubic polynomial baseline. Quantum yields were determined by interactively subtracting a variable fraction of the 8 K ligand-bound spectrum (MbO_2) from the 8 K photolyzed spectrum (Mb^*O_2) until the contribution to the difference spectrum at the peak wavelength of the ligand-bound spectrum was zero (i.e., at 418 nm for MbO_2 and 426 nm for $CoMbO_2$) (Figure 1). The value of the variable fraction that satisfies this condition was the fraction of ligand-bound material that remained in the Mb^*O_2 spectrum after photolysis. Therefore, the photolysis quantum yield was obtained by subtracting that fraction from 1.0. The difference spectrum that remained after subtracting $(1 - QY) \times MbO_2$ from Mb^*O_2 was that of the MbO_2 photoproduct (Mb^*+O_2). Second derivatives were taken of the MbO_2 and Mb^*O_2 spectra to aid in identifying peak positions and the number of components in each spectrum. One must keep in mind that any positive peaks in the raw spectrum will appear as negative peaks in the second derivative spectrum.

X-ray Absorption Spectra. X-ray absorption spectra were collected at the National Synchrotron Light Source (NSLS) at Brookhaven National Laboratory, on beamline X9B with a sagittally focused Si(111) crystal monochromator with fixed exit geometry. 4 mrad horizontal acceptance of the X-ray beam was horizontally focused to 4.0 mm; the horizontal and the vertical apertures were set to 1.0 and 0.25 mm, respectively, yielding a photon flux of 8×10^9 s^{-1} on the sample. K_α fluorescence was detected with a 13-element

germanium detector (Cramer et al., 1988) (Canberra) interfaced to a PDP 11/23+ computer. An iron or cobalt foil was used as a reference to account for any shifts in the monochromator. The reference signal was generated by scattering X-ray photons off of a piece of kaypton tape mounted 45° to the X-ray beam and through the metal foil; the fluorescence was detected by a zinc sulfide coated photomultiplier tube oriented 90° to the X-ray beam. A protocol for data collection was chosen keeping in mind that typical differences in X-ray edge positions between oxy- and deoxymyoglobin species are 2−3 eV and the width of each LFIR peak is ~30 eV. Thus, high-resolution spectra were obtained by collecting data points in 0.5 eV steps (2 s/pt integration time) across the X-ray edge, and 1.0 eV steps (4 s/pt integration time) through the X-ray absorption near edge (XANES) region.

Samples were mounted in copper sample holders with mylar windows (10 mm wide × 5 mm high × 0.5 mm thick) and frozen in liquid nitrogen. The frozen samples were mounted in a closed-cycle helium displex and cooled to 20 K. For the photoproduct spectra, samples were photolyzed using a Nd:YAG laser (Surelite, Continuum) that was frequency-doubled to 532 nm, with an average power of 40 mW and 10 Hz repetition rate (i.e., 4 mJ/pulse). The laser beam diameter was 6 mm. The photolysis protocol was first tested with an MbCO sample, which is fully photolyzable; 100% photolysis was achieved, indicated by a 2.5 eV shift in X-ray edge position and a change in the ligand field indicator region ratio from 0.70 to 1.30 (Chance, 1986; Chance et al., 1986).

X-ray edge positions are defined by the peak of the spectrum's first derivative (Belli et al., 1980; Wong et al., 1984; Wirt et al., 1991). In order to obtain the ligand field indicator ratio (LFIR), the LFIR region was first fit to a cubic polynomial baseline between the minimum point preceding the first LFIR peak and the tail following the second LFIR peak (see Figure 2). Then, perpendiculars are erected from the horizontal baseline to the two peaks, A and B. The LFIR ratio is defined as the height of peak A divided by the height of peak B (B. Chance et al., 1984; M. Chance et al., 1986; Chance, 1986). The error in the LFIR ratio is determined by reproducibility from scan to scan and from different preparations. A total of 6−10 scans were taken for each sample, and 2−3 preparations were made of each sample. This analysis, though empirical, has a high predictive value and is especially valuable in examining changes in metal displacement or differences among closely related compounds (Bianconi et al., 1984; Shiro et al., 1991). A more thorough, quantitative approach using FEFF 6.0 is underway and supports the empirical approach (J. Rehr and M. Chance, unpublished observations).

RESULTS AND DISCUSSION

Low Temperature Quantum Yields of Photolysis: A Measure of the Inner Barrier to Oxygen Binding. Ligands such as NO, O_2, and CO have similar outer barrier for ligand binding, and the variations in k_{on} for these species come from different inner barriers (Doster et al., 1982; Carver et al., 1990; Gibson et al., 1992). The inner barrier to ligand binding can be isolated at cryogenic temperatures (Austin et al., 1975), and the magnitude of this barrier can be probed through the low temperature quantum yield of photolysis, where higher inner barriers result in higher photoproduct yields (Chance et al., 1990). An investigation of the low temperature quantum yields of photolysis for $FeMbO_2$ and $CoMbO_2$ directly addresses the effect of metal substitution on the inner rebinding barrier.

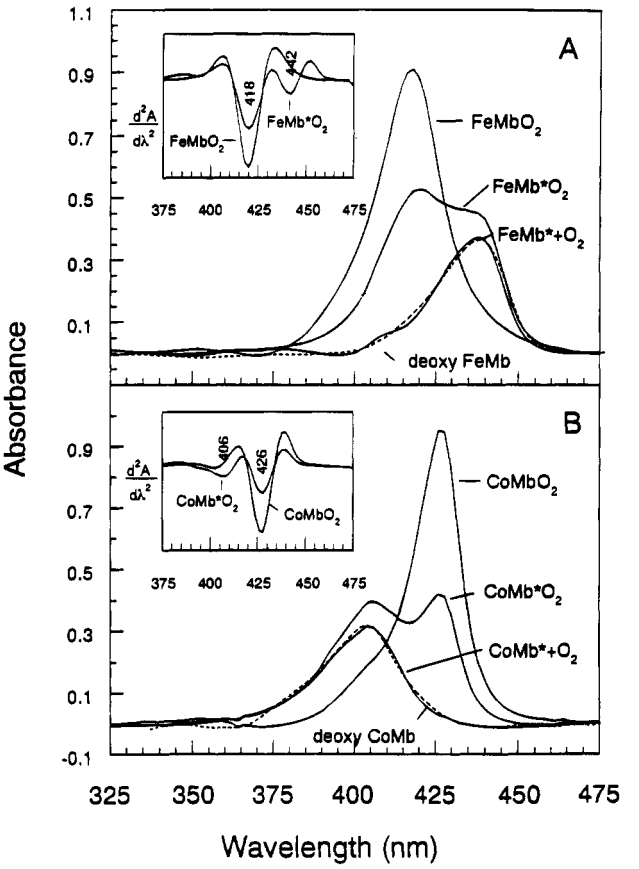

FIGURE 1: Optical spectra at 10 K for the following species: (A) ligand-bound ($FeMbO_2$), photolyzed ($FeMb^*O_2$), deduced photoproduct ($FeMb^*+O_2$), and deoxy (deoxy-FeMb) ferrous myoglobin and (B) ligand-bound ($CoMbO_2$), photolyzed ($CoMb^*O_2$), deduced photoproduct ($CoMb^*+O_2$), and deoxy (deoxy-CoMb) cobaltous myoglobin. The $CoMbO_2$ and $FeMbO_2$ samples were both 1.4 mM, pH 7.0. For each spectrum, data collection time was 0.1 s with 2 nm resolution. Samples were photolyzed for 5 min per side using a high-intensity white light source or by a 2 min exposure to the spectrometer's deuterium lamp.

A comparison of the 8 K ligand-bound (MbO_2), photolyzed (Mb^*O_2), observable photoproduct (Mb^*+O_2), and deoxy optical spectra of CoMb and FeMb can be seen in Figure 1. Insets to Figure 1 include second derivative spectra of MbO_2 and Mb^*O_2 for defining peak positions and the number of components in each spectrum. Ligand-bound MbO_2 is composed of a single peak with a maximum at 418 nm for $FeMbO_2$, and 426 nm for $CoMbO_2$. [The small shoulder at 406 nm in the $CoMbO_2$ spectrum is due to a small amount (~5%) of deoxy CoMb in the sample.] The Mb^*O_2 spectra each contain two components—one with a maximum at the position of ligand-bound MbO_2 and the second with a maximum at the position of deoxy-Mb. Both $CoMb^*+O_2$ and $FeMb^*+O_2$ are extremely similar to their corresponding deoxy species.

The $FeMb^*+O_2$ spectrum was obtained by subtracting 0.50 × $FeMbO_2$ from the $FeMb^*O_2$ spectrum. This result indicates that 50% of the $FeMb^*O_2$ spectrum is due to ligand-bound $FeMbO_2$, indicating a photolysis quantum yield of 0.50 ± 0.05, which is within the error of similar studies by Chance et al. (0.4 ± 0.1), which were also taken at much higher

resolution (0.4 nm) (Chance et al., 1990). This shows the Hewlett Packard system gives data comparable to a high resolution diode array setup. In the same fashion, the CoMb*+O_2 spectrum was generated by subtracting 0.45 × $CoMbO_2$ from the CoMb*O_2 spectrum, indicating 45% of the CoMb*O_2 spectrum is due to ligand-bound $CoMbO_2$, giving a photolysis quantum yield of $CoMbO_2$ of 0.55 ± 0.05. Within the error of our measurements, the photolysis quantum yields of $CoMbO_2$ and $FeMbO_2$ are the same. This result supports the theory that $CoMbO_2$ and $FeMbO_2$ have similar inner barriers to oxygen binding, suggested by similar values for k_{on}.

The Proximal Barrier to Ligand Binding and Metal−Heme Displacement. The geminate barrier to oxygen binding can be divided into proximal and distal barriers (Bertini et al., 1994). Proximal barriers involve the stereochemistry of the metalloporphyrin and coordination of the proximal histidine. Distal barriers arise from noncovalent interactions of the metalloporphyrin and the dioxygen ligand with the surrounding solvent and protein. The magnitude of the proximal barrier to ligand binding is influenced by the displacement of the iron from the heme plane, where ligands that rebind to a nonplanar heme have a lower barrier than those which rebind to a planar heme (Chance et al., 1990). X-ray crystallographic and X-ray absorption studies have shown that for ligand-bound MbCO, the iron is oriented in the heme plane (Chance, 1986; Chance et al., 1986; Kuriyan et al., 1986); for ligand-bound MbO_2, the iron is displaced 0.2 Å from the heme plane (Phillips, 1980; Chance, 1986; Chance et al., 1986); and for deoxy-Mb, the iron is even further displaced from the heme plane (0.35 Å) (Phillips, 1981). Photolysis results in the motion of the metal from its ligand-bound position toward a deoxy-like conformation, and rebinding requires motion of the metal back toward the heme plane. Since O_2 may recombine more easily to a nonplanar heme, where MbCO recombines to a planar heme, low-barrier or barrierless recombination is more probable for MbO_2 than MbCO (Chance et al., 1990). Thus, a comparison of the metal−heme displacements in deoxy, oxy, and the low temperature photoproduct of CoMb and FeMb provides valuable information on a measure of the proximal barrier to oxygen binding in the two species.

X-ray absorption near edge spectroscopy (XANES) is an excellent technique for examining the metal displacement (M−Ct) from the heme plane in the deoxy, photoproduct, and ligand-bound forms of hemeproteins. Chance and co-workers (B. Chance et al., 1984; M. Chance et al., 1986; Chance, 1986) have shown that the ratio of peaks in the ligand field indicator region (LFIR) of a XANES spectrum (Figure 2) can be correlated to the spin state and iron out-of-plane distance in ferryl, ferric, and ferrous hemeproteins. Changes in the LFIR are seen to arise from changes in the backscattering of higher shell ligands. LFIR changes arise from focusing effects, which are important when backscattering atoms are in line with the absorbing metal atom. The LFIR regions of the $CoMbO_2$, CoMb*O_2, and deoxy-CoMb X-ray absorption spectra are illustrated in Figure 2. The relationship between the LFIR ratio and M−Ct (as determined by X-ray crystallography) for various myoglobin compounds is shown in Figure 3. As can be seen, the relationship follows the least-squares line: LFIR = (M−Ct × 2.3) + 0.66. A summary of the LFIR ratios and M−Ct

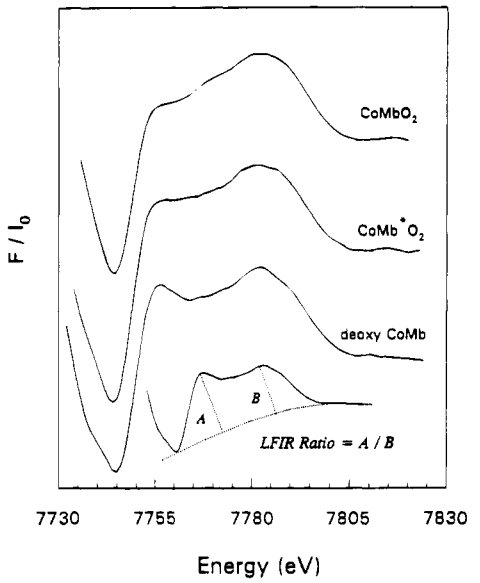

FIGURE 2: Ligand field indicator region (LFIR) of the X-ray absorption of $CoMbO_2$, CoMb*O_2, and deoxy-CoMb. The LFIR ratio is defined as the height of peak A divided by the height of peak B (see text for details). Both the $CoMbO_2$ sample and the deoxy-CoMb samples were 1 mM, pH 7.0. Spectra were obtained by collecting data points in 1.0 eV steps with 4 s/pt integration time. Samples were photolyzed at 20 K with a frequency-doubled Nd:YAG laser (4 mJ/pulse) throughout the scan.

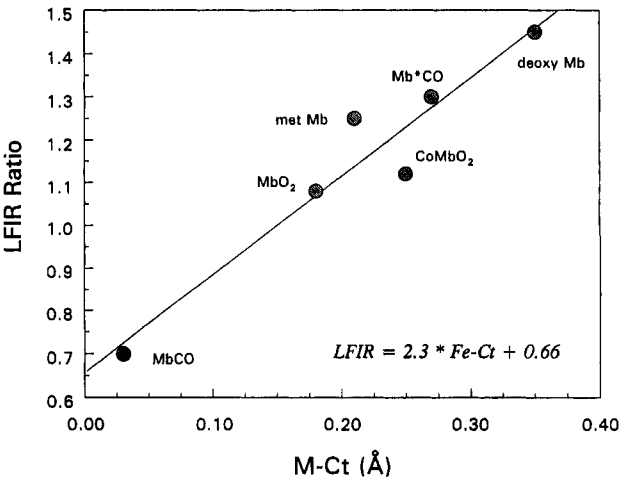

FIGURE 3: Correlation of the LFIR ratio with the metal displacement (M−Ct) of various myoglobin species as determined by X-ray crystallography. The estimated error in the LFIR ratio values is ±0.05. The equation for the least-squares line is LFIR = (2.3 × M−Ct) + 0.66.

distances for both the ferrous and cobaltous myoglobin species can be found in Table 2.

X-ray crystallographic studies show that the metal−heme displacement of $CoMbO_2$ (Petsko et al., 1978) resembles $FeMbO_2$ (Phillips, 1980). Within the error of the measurement, the LFIR ratios for $CoMbO_2$ (1.12 ± 0.05) and $FeMbO_2$ (1.08 ± 0.05) are the same, indicating similar metal displacements from the heme plane, in agreement with the crystallographic data. For the deoxy species, X-ray crystallographic data for deoxy-meso-CoMb (Padlan et al., 1975), deoxy-CoHb (Fermi et al., 1982), and several five-coordinate cobaltous heme model compounds (Scheidt & Hoard, 1973; Fermi et al., 1982) predict a metal displacement for deoxy-CoMb which is slightly less than or equal to that of deoxy-FeMb (Phillips, 1981). Analogously, the LFIR ratios for

Table 2: X-Ray Absorption Edges and LFIR Ratios for Ferrous and Cobaltous Myoglobin

	X-ray absorption edge (eV)[a,c]	LFIR ratio[b,c]	M−Ct (Å)[e] (XAS-LFIR)[f]	M−Ct (Å)[e] (crystallography)
$FeMbO_2$	7125.0	1.08	0.18	0.18[g]
$FeMb^*O_2$		1.24[c]		
$FeMb^*+O_2$		1.40[d]	0.32	
deoxy-Mb	7122.0	1.45	0.34	0.35[h]
$CoMbO_2$	7723.5	1.12	0.20	0.25[i]
$CoMb^*O_2$		1.25[c]		
$CoMb^*+O_2$		1.36[d]	0.31	
deoxy CoMb	7721.5	1.36	0.31	
MbCO	7124.5	0.70[j]	0.02	0.03[k]
Mb*CO		1.30[j]	0.28	0.27[l]
				0.25[m]

[a] X-ray edge positions determined assuming values for an iron foil of 7111.0 eV and cobalt foil of 7709.0 eV; errors on X-ray edge positions are ±0.2 eV. [b] Errors on LFIR ratios are ±0.05. [c] Experimental results uncorrected for photolysis quantum yield. [d] Calculated results corrected for photolysis quantum yield: $FeMbO_2$, 0.50 ± 0.05; $CoMbO_2$, 0.55 ± 0.05. [e] Metal displacement from the mean heme plane. [f] Calculated from LFIR = (M−Ct × 2.3) + 0.66. Errors are ±0.07 Å. [g] Phillips (1980). [h] Phillips (1981). [i] Petsko, et al. (1978). [j] Chance (1986). [k] Kuriyan et al. (1986). [l] Schlichting et al. (1994). [m] Srajer et al. (1988).

deoxy-CoMb (1.36 ± 0.05) and deoxy-FeMb (1.45 ± 0.05) indicate very similar metal displacements for the two species.

Crystallographic data are not available for the low temperature $CoMbO_2$ and $FeMbO_2$ photoproducts, but we are able to assess the degree of metal displacement using the LFIR ratios for the two species. Since the quantum yield of photolysis of MbO_2 is less than unity, the LFIR spectrum of Mb^*O_2 contains 50% of ligand-bound material (MbO_2) and 50% photolyzed material (Mb^*+O_2). Thus, in order to determine the LFIR ratio of the photolyzed part (Mb^*+O_2) of the Mb^*O_2 spectrum, we have used the following linear combination equation, which incorporates the quantum yield of photolysis for MbO_2. It should be noted that this method assumes that the "unphotolyzable" population of MbO_2 has an LFIR ratio that is indistinguishable from that of liganded MbO_2:

$$LFIR_{Mb^*O_2} = [LFIR_{Mb^*+O_2}QY] + [LFIR_{\text{liganded } MbO_2}(1 - QY)]$$

Table 2 contains both the uncorrected LFIR ratios and the quantum yield-corrected values. As can be seen, the metal displacements for the observed photoproduct populations are indistinguishable from each other and the corresponding deoxy species ($CoMb^*+O_2$: 1.36 ± 0.05; $FeMb^*+O_2$: 1.40 ± 0.05). This result is in contrast to the LFIR ratio of the MbCO photoproduct (1.30), in which the iron displacement is only ~75% of the deoxy-Mb iron displacement (1.45) (Chance, 1986; Powers et al., 1987). The mean displacement for the MbCO photoproduct is supported by crystallographic data (Schlichting et al., 1994) and theoretical calculations (Srajer et al., 1988). Finally, it is important to note that XANES describes only an average displacement while the actual situation is assumed to consist of a population of substates with a mean value reflected in the XANES result. In the case of $CoMbO_2$ and $FeMbO_2$, where the quantum yields of photolysis are less than unity, the photoproduct results reveal only the *observed* photoproduct; we cannot directly examine the structure of the presumably fast rebinding species, i.e., the fraction of MbO_2 molecules (~50%) with essentially zero barrier to rebinding.

In summary, these XANES results (Table 2) indicate that both ligand-bound $CoMbO_2$ and $FeMbO_2$ have metal−heme displacements of ~0.2 Å, which is different from MbCO, in which iron is located in the mean heme plane. Also, the observed photoproducts of MbCO and MbO_2 are different, the latter being more "deoxy-like".

The Distal Barriers to Oxygen Release and the Electron Reorganization through the Metal−Dioxygen Moiety upon Oxygenation. The ~300-fold increase in the rate of oxygen dissociation (k_{off}) for $CoMbO_2$ (Yamamoto et al., 1974) versus $FeMbO_2$ (Antonini & Brunori, 1971) suggests considerable differences in the barriers to oxygen release for the two species. Studies on distal pocket myoglobin mutants have indicated that k_{off} is influenced by distal pocket effects, i.e., the structural and electronic changes that occur in the M−O−O moiety itself and its interaction with the distal pocket residues upon oxygenation (Carver et al., 1990; Rohlfs et al., 1990; Lee et al., 1994). The strengths of the M−O and O−O bonds, polarity of the M−O−O unit, distal pocket polarity, and hydrogen bond strength are all contributing factors to individual barriers to oxygen binding and release in myoglobin.

X-ray Edge Positions. Early infrared studies provided direct evidence for transfer of electron density from the metal to the dioxygen ligand in $CoMbO_2$ and $FeMbO_2$ (Barlow et al., 1973; Maxwell & Caughey, 1974; Maxwell et al., 1974). Numerous electron paramagnetic resonance (EPR) studies on deoxy-CoMb, $CoMbO_2$, and the $CoMbO_2$ photoproduct have also shown that there is a significant transfer of the unpaired electron density from cobalt to the ligand upon oxygenation; however, the g values are not indicative a full Co(III)−O_2^- structure (Hoffman & Petering, 1970; Chien & Dickinson, 1972; Yonetani et al., 1974a; Hori et al., 1982; Ikeda-Saito et al., 1977, 1991; Lee et al., 1992, 1994). A direct comparison cannot be made to native oxymyoglobin because it has a diamagnetic iron and is, thus, EPR-inactive. Nonetheless, similar conclusions have been drawn from Mossbauer spectroscopy on FeMb, $FeMbO_2$, and the $FeMbO_2$ photoproduct (Spartalian et al., 1976).

The X-ray absorption edge position also provides a measure of relative metal−ligand electron density distributions. In this case, its advantage over EPR is that this technique can be used to directly compare CoMb and FeMb. Numerous studies have correlated the position of the X-ray edge to the effective charge on the central metal, i.e., the energy required to remove a K-shell electron decreases as the effective charge on the central metal becomes more negative (Belli et al., 1980; Wong et al., 1984; Wirt et al., 1991; Scheuring et al., 1994). Shifts in the X-ray edge position as a ligand binds implies a reorganization of electron density between the metal and the ligand. Table 2 contains the X-ray edge positions of the oxy- and deoxy- forms of cobaltous and ferrous myoglobin. As oxygen binds, the X-ray edge positions of both FeMb and CoMb shift to higher energy (FeMb, 7122 eV; $FeMbO_2$, 7125 eV; CoMb, 7721.5 eV; $CoMbO_2$, 7723.5 eV), implying a decreased electron density on the metal and transfer of that electron density to the ligand and/or to the porphyrin ring.

Comparison of the X-ray edge positions of the six-coordinate ligand-bound oxy species to six-coordinate models

of the M(III) oxidation states [ferric: met Mb, 7126.0 eV, data not shown; cobaltic: cobalt(III) hexamine and aquocobalamin, 7724.0 eV (Wirt et al., 1993)] indicate that in neither case is the electron reorganization consistent with a full M(III)$-O_2^-$ species.

The importance of these results lies in the ability to use the same technique to directly address the redistribution of electron density upon oxygenation of CoMb and FeMb. The energy required for maximal electron transfer from the M(II) state to the M(III) state is 4 eV for iron and 2.5 eV for cobalt. Thus $CoMbO_2$ has 80% of the maximal electron transfer to oxygen (2 out of 2.5 eV) and $FeMbO_2$ has 75% (3 out of 4 eV), implying similar relative degrees of electron transfer when oxygen binds to either species.

The Metal−Oxygen Bond. Although both cobalt and iron transfer similar electron density to the ligand upon oxygenation, the distribution of this electron density throughout the M−O−O moiety and its effect on the distal barriers to oxygen binding and release are not necessarily the same. Resonance Raman studies of $CoMbO_2$ and $FeMbO_2$ (Tsubaki & Yu, 1981; Tsubaki et al., 1982) have established that ν(Co−O) falls at ~540 cm^{-1} whereas ν(Fe−O) falls at ~570 cm^{-1}. Lower Co−O versus Fe−O stretching frequencies have also been observed for cobaltous and ferrous model compounds such as "picket fence" porphyrins [$M(O_2)(T_{piv}PP)(1MeIm)$] (Walters et al., 1980; Proniewicz et al., 1989). Since Co−O−O and Fe−O−O have similar geometries (Petsko et al., 1978; Phillips, 1980), and the mass effect predicts only a ~4 cm^{-1} shift, the ~30 cm^{-1} difference has been attributed to a weakening of the Co−O bond relative to the Fe−O bond (Tsubaki & Yu, 1981; Tsubaki et al., 1982). A higher dissociation rate constant (k_{off}) for $CoMbO_2$ versus $FeMbO_2$ (Yamamoto et al., 1974; Tsubaki & Yu, 1981) and a lower oxygen affinity ($P_{0.5}$) for $Co(O_2)(T_{piv}PP)$-(1MeIm) versus $Fe(O_2)(T_{piv}PP)(1MeIm)$ (Collman et al., 1978) are thought to arise from these weaker Co−O bonds.

The origin of a weaker Co−O bond appears to lie in the electronic configuration of the Co−O−O unit. Upon oxygenation of the cobaltous porphyrin, significant unpaired electron density is transferred from the cobalt d_{z^2} orbital to a π^* antibonding molecular orbital, localized on oxygen (Hoffman & Petering, 1970; Chien & Dickinson, 1972; Wayland et al., 1974; Yonetani et al., 1974b; Tsubaki & Yu, 1981). For $FeMbO_2$, where there is one less d-electron to populate the molecular orbital scheme, this π^* orbital is vacant. This vacancy promotes stronger π-bonding in the $FeMbO_2$ case and is supported by a higher ν(M−O) for $FeMbO_2$ (Wayland et al., 1974; Tsubaki & Yu, 1981).

The Bound-Dioxygen Bond. Resonance Raman spectroscopy has been the technique of choice in probing the dioxygen stretching frequency, ν(O−O), of $CoMbO_2$ (Tsubaki & Yu, 1981; Bruha & Kincaid, 1988; Proniewicz & Kincaid, 1990), although one infrared study has also been reported (Maxwell & Caughey, 1974). Unlike ferrous oxymyoglobin, Yu and co-workers have shown that ν(O−O) in $CoMbO_2$ is resonance enhanced by excitation at 406.7 nm (Tsubaki & Yu, 1981). Since then, several RR studies (Tsubaki & Yu, 1981; Bruha & Kincaid, 1988; Proniewicz & Kincaid, 1990) have revealed a multiple-band pattern in the dioxygen-stretch region. Through an elaborate study of cobaltous myoglobin and hemoglobin, and several cobalt porphyrin model compounds, Kincaid and co-workers (Bruha & Kincaid, 1988; Proniewicz & Kincaid, 1990) have attributed the multiple band pattern to coupling of ν(O−O) to internal modes of the proximal and/or distal histidine. They identified the inherent ν(O−O) at ~1135 cm^{-1}.

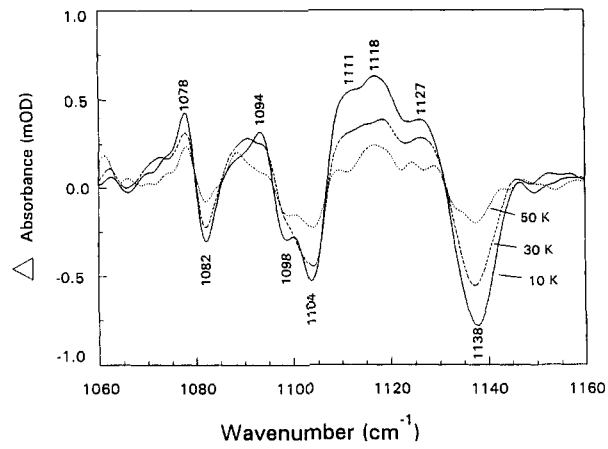

FIGURE 4: Difference FTIR spectra (photolyzed/unphotolyzed) of $CoMb^{16}O_2$ at 10, 30, and 50 K. Spectra were generated by taking the ratio of the photoproduct $CoMbO_2$ spectrum and the ligand-bound $CoMbO_2$ spectrum at each respective temperature and adjusting the baseline of the resultant spectra with a cubic polynomial. As the sample is warmed, oxygen rebinds and the differences between the photoproduct and ligand-bound spectra decrease. The $CoMb^{16}O_2$ sample was 2.5 mM, pH 7.0. The sample thickness was 0.0025 cm. Both samples were photolyzed with a high-intensity white light source for 5 min per side. For each spectrum, 128 scans were taken at 2 cm^{-1} resolution.

Infrared spectroscopy has been the primary means of investigating the dioxygen stretch in ferrous oxymyoglobin (Barlow et al., 1973; Maxwell & Caughey, 1974; Maxwell et al., 1974; Potter et al., 1987). Similar to the Raman results for $CoMbO_2$, Caughey and co-workers (Potter et al., 1987) observe several modes in the dioxygen stretch region that are sensitive to isotopically labeled O_2. They propose that the multiple-band pattern is attributable to two $FeMbO_2$ conformational substates, the lower of which is split by an unidentified perturbation. If unperturbed, ν(O−O) would fall at ~1120 and ~1150 cm^{-1}.

Recently, we took advantage of the photolyzability of MbO_2 and generated infrared difference spectra of photolyzed/unphotolyzed $FeMbO_2$ at 10 K (Miller & Chance, 1994). The resulting spectra revealed several photolysis-sensitive modes in the dioxygen stretch region that are due to conformational changes which occur in the heme peripheral vinyl groups and the proximal histidine as MbO_2 is photolyzed. In agreement with the theory of Kincaid and co-workers (Bruha & Kincaid, 1988; Proniewicz & Kincaid, 1990), these heme and proximal histidine modes couple with ν(O−O).

In this paper, we present the results of a similar experiment using $CoMbO_2$ (Figure 4). The 10 K $CoMbO_2$ difference spectrum is obtained by dividing the photoproduct $CoMbO_2$ spectrum at 10 K by the ligand-bound $CoMbO_2$ spectrum at 10 K, i.e., $CoMb^*O_2$ (10 K)/$CoMbO_2$ (10 K). Similar difference spectra are obtained at 30 and 50 K. As the sample recombines, the differences between $CoMb^*O_2$ and $CoMbO_2$ are reduced. All negative peaks are features of ligand-bound MbO_2 and the positive peaks are characteristics of the MbO_2 photoproduct. Positive peaks at 1078 and 1094 cm^{-1} and negative peaks at 1082 and 1098 cm^{-1} are attributed to modes of the heme peripheral vinyl groups (Miller & Chance, 1994). The negative peak at 1104 cm^{-1}

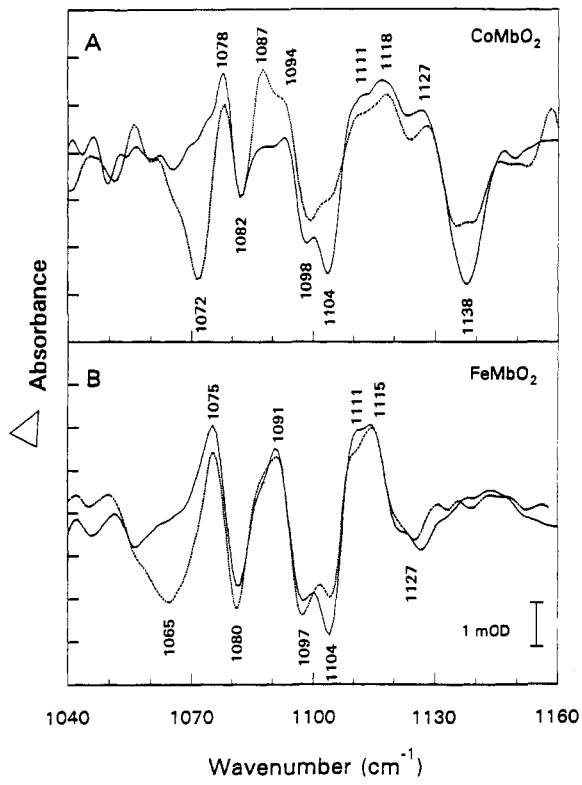

FIGURE 5: Difference FTIR spectra (photolyzed/unphotolyzed) of (A) $CoMb^{16}O_2$ (—) versus $CoMb^{18}O_2$ (---) at 10 K and (B) $FeMb^{16}O_2$ (—) versus $FeMb^{18}O_2$ (---) at 10 K. The $CoMb^{16}O_2$ sample was 2.5 mM, pH 7.0. The $CoMb^{18}O_2$ sample was 1.8 mM, pH 7.0. The $FeMb^{16}O_2$ sample was 4.3 mM, pH 6.0. The $FeMb^{18}O_2$ sample was 7.7 mM, pH 6.0. Spectra collection, sample photolysis, and data analysis protocols are described in the legend to Figure 4.

and positive peak at 1111 cm^{-1} have been assigned to a C—H bending mode of the proximal histidylimidazole. A small contribution to the negative intensity at 1104 cm^{-1} is due to ν(O—O). These features of the $CoMbO_2$ difference spectrum are very similar to $FeMbO_2$ (Miller & Chance, 1994) (Figure 5). An outstanding difference between the spectra of $CoMbO_2$ and $FeMbO_2$ is the intense negative peak at 1138 cm^{-1} in the $CoMbO_2$ spectrum, which is absent in the $FeMbO_2$ spectrum.

Figure 5A illustrates that this band is sensitive to dioxygen isotopic substitution. A 10 K photolyzed/unphotolyzed difference spectrum of $CoMb^{18}O_2$ reveals a decreased intensity of the 1138 cm^{-1} mode and an intense new negative peak at 1072 cm^{-1}. There is also a small intensity decrease at 1104 cm^{-1} in the $CoMb^{18}O_2$ spectrum. The expected isotopic shift when replacing $^{16}O_2$ with $^{18}O_2$ is a decrease in frequency of ~65 cm^{-1} (Bajdor et al., 1984; Kincaid et al., 1985). These results suggest that the 1138 cm^{-1} mode is $\nu(^{16}O-^{16}O)$, which shifts to 1072 cm^{-1} with $^{18}O_2$ substitution. (The remaining intensity at 1138 cm^{-1} in the $CoMb^{18}O_2$ spectrum is due to a small amount of $^{16}O_2$ in the sample.)

The isotopic sensitivity of the 1104 cm^{-1} mode can be explained by a coupling of the inherent $\nu(^{16}O-^{16}O)$ at ~1138 cm^{-1} to the 1107 cm^{-1} mode of the proximal histidine (Bruha & Kincaid, 1988; Proniewicz & Kincaid, 1990; Miller & Chance, 1994), resulting in perturbed modes at 1138 and 1104 cm^{-1} with O_2 and proximal histidine character. The position of ν(O—O), its isotopic sensitivity, and its coupling to modes of the heme—histidylimidazole moiety, which we have obtained here through IR spectroscopy, are in agreement with the earlier RR studies of $CoMbO_2$ by Kincaid and co-workers (Bruha & Kincaid, 1988; Proniewicz & Kincaid, 1990).

For a direct comparison of the dioxygen stretch between $CoMbO_2$ and $FeMbO_2$, the 10 K photolyzed/unphotolyzed difference spectra of $FeMb^{16}O_2$ and $FeMb^{18}O_2$ can be seen in Figure 5B. The $^{18}O_2$ spectra are relatively straightforward. The $CoMb^{18}O_2$ and $FeMb^{18}O_2$ spectra are alike except that the peak identified as $\nu(^{18}O-^{18}O)$ at 1072 cm^{-1} in the $CoMb^{18}O_2$ spectrum falls at 1065 cm^{-1} in the $FeMb^{18}O_2$ spectrum, implying that the dioxygen stretch for $FeMbO_2$ is ~7 cm^{-1} lower than for $CoMbO_2$. Similar to our results for $FeMb^{18}O_2$, Caughey and co-workers (Potter et al., 1987) identified an intense feature at 1065 cm^{-1} in the infrared spectrum of $FeMb^{18}O_2$, which they attributed to $\nu(^{18}O-^{18}O)$.

The $Mb^{16}O_2$ spectra are more complex. The ν(O—O) mode corresponding to the 1138 cm^{-1} mode in the $CoMb^{16}O_2$ spectrum is missing from the $FeMb^{16}O_2$ spectrum, but the photolysis-sensitive vinyl and histidine modes are essentially the same and the isotopic sensitivity at 1105 cm^{-1} is still present. Caughey and co-workers (Potter et al., 1987) also observe isotopic sensitivity at 1105 cm^{-1} for $FeMbO_2$ which is lower than the expected $^{18}O_2 \rightarrow {}^{16}O_2$ isotopic shift. They attribute it to coupling of the "real" ν(O—O), which appears as an extremely weak mode around ~1127 cm^{-1}, to an unidentified perturbation, which we have identified as a proximal histidine mode at 1107 cm^{-1} (Miller & Chance, 1994).

This model by Caughey and co-workers provides a reasonable explanation of the data; however, some issues still remain unclear from this interpretation. For example, the coupling of ν(O—O) in $FeMb^{16}O_2$ appears to be weak, as evidenced by the small (2 cm^{-1}) shift of the 1107 cm^{-1} histidine mode. So, the expected perturbation of ν(O—O) should not be as complex as it appears. Also, the sum of the intensities of the perturbed modes at 1105 and 1127 cm^{-1} is weaker than $\nu(^{18}O-^{18}O)$ at 1065 cm^{-1} (Potter et al., 1987). The data presented here are consistent with that finding. Although weak coupling of two modes may result in a redistribution of intensity, the total intensity is expected to remain constant.

In summary, ν(O—O) of $CoMb^{18}O_2$ falls at 1072 cm^{-1} and shifts by 66 cm^{-1} in $CoMb^{16}O_2$ to 1138 cm^{-1}. Conversely, the dioxygen stretching frequency of $FeMb^{18}O_2$ falls at 1065 cm^{-1}. The unperturbed dioxygen stretching frequency in $FeMb^{16}O_2$ is not observed, but using the predicted (calculated) isotopic shift of ~66 cm^{-1}, which is also the observed isotopic shift for $CoMbO_2$, we predict the dioxygen stretch of $FeMb^{16}O_2$ to fall at ~1131 cm^{-1}. Thus, our results agree with Kincaid and co-workers that ν(O—O) falls at ~1138 cm^{-1} in $CoMb^{16}O_2$, and we propose that ν(O—O) falls at ~1131 cm^{-1} in $FeMb^{16}O_2$.

Implications for M—O—O Polarity, Distal Pocket Polarity, and Hydrogen Bond Strength. The kinetics of oxygen binding and release for distal histidine mutants of $FeMbO_2$ and $CoMbO_2$ reveal increased O_2 affinities for those mutants with polar distal residues (Carver et al., 1990; Rohlfs et al., 1990; Ikeda-Saito et al., 1991). ESEEM studies of these $CoMbO_2$ mutants demonstrate a direct relationship between the ionic character of the Co—O—O moiety and the polarity of the distal residue (Lee et al., 1994). Rohlfs et al. (1990) have proposed that oxygen affinity is controlled by the ability of the distal residue to stabilize a polar M—O—O unit, most

notably by forming a hydrogen bond to the bound dioxygen. Thus the polarity of the M−O−O moiety may be a deciding factor in the ~300-fold increase in k_{off} for $CoMbO_2$ versus $FeMbO_2$.

The polarity of the M−O−O unit is dependent on its electronic structure, i.e., how the pair of σ-bonding electrons is distributed and on the degree of π-backbonding from the O−O region to the M−O bonding region (Wayland et al., 1974; Reed & Cheung, 1977). Structurally, bending of the M−O−O moiety tends to localize the σ-bonding electron pair on oxygen, approaching $M(III)-O_2^-$, and decreasing backbonding. Both MbO_2 (115°) (Phillips, 1980) and $CoMbO_2$ (131°) (Petsko et al., 1978) are significantly bent, implying highly polar ($M^{III}O_2^-$) species. Even though it is bent, considerable π-backbonding still occurs in MbO_2 because the Fe^{III} species ($3d^5$) has a half-filled d_{xz} orbital that is expected to accept π-electron density back from O_2^-. In contrast to MbO_2, the backbonding from O_2^- in $CoMbO_2$ is substantially less than MbO_2 because the Co^{III} species ($3d^6$) has a filled d_π^6 configuration (Wayland et al., 1974; Reed & Cheung, 1977). Decreasing backbonding tends to decrease ν(M−O) and increase ν(O−O). A lower value for ν(M−O) for $CoMbO_2$ is consistent with less backbonding for this species and supports a higher value for k_{off}.

Studies on MbCO by Spiro and co-workers have shown that polar interactions between the terminal $O^{\delta-}$ atom of CO and the distal pocket residue(s) tend to stabilize the developing negative charge on the terminal O atom produced by the backbonding (Li & Spiro, 1988; Hu et al., 1994; Ray et al., 1994). The net effect is an increase in backbonding. This effect is very dramatic where there is a hydrogen bond to the ligand, as in the case of low-pH CO−horseradish peroxidase (Uno et al., 1987) and low-pH CO−cytochrome *c* peroxidase (Smulevich et al., 1986). Analogous to the case for MbCO, backbonding is expected to be especially strong in MbO_2 at pH 7, where there is a hydrogen bond between the distal histidine and the oxygen ligand.

In model systems where the distal-side hydrogen bond is absent, such as ferrous and cobaltous "picket fence" porphyrins (Collman et al., 1975), the dioxygen stretch is significantly higher when compared to $FeMbO_2$ and $CoMbO_2$ at pH 7, where the distal-side hydrogen bond is present. It falls at 1150 cm^{-1} in $Co(O_2)(T_{piv}PP)(1MeIm)$ and 1159 cm^{-1} in $Fe(O_2)(T_{piv}PP)(1MeIm)$ (Collman et al., 1976). This supports the theory by Spiro and co-workers that positive polar interactions increase backbonding, i.e., decrease ν(O−O). The difference in frequency between the non-hydrogen-bonded model and the hydrogen-bonded protein is significantly less for $CoMbO_2$ (~12 cm^{-1}) as compared to MbO_2 (~28 cm^{-1}). This result suggests that formation of the hydrogen bond in $FeMbO_2$ provides a greater effect on the distribution of electron density throughout the M−O−O···HN moiety, potentially suggesting a stronger hydrogen bond to the distal histidine, and stabilizing a more polar Fe−O−O bond, thus increasing its oxygen affinity.

CONCLUSIONS

Substitution of cobalt for iron in myoglobin results in physiological rates of oxygen association (k_{on}) to CoMb and FeMb that are similar and physiological rates of oxygen dissociation (k_{off}) from $CoMbO_2$ and $FeMbO_2$ that are different. Relative values for k_{on} and k_{off} are a measure of the size of the overall (distal and proximal) barriers to oxygen binding and release, respectively, suggesting that CoMb and FeMb have similar barriers to oxygen binding and unique barriers to oxygen release. We have identified both structural and electronic similarities and differences between CoMb and FeMb that may contribute to these barriers.

A correlation has been observed between the low temperature quantum yields of photolysis and the overall barrier to ligand binding. Thus, photolysis yields provide a spectroscopic measure of relative values for k_{on}. We observe this trend in similar quantum yields of photolysis for $CoMbO_2$ (0.55 ± 0.5) and $FeMbO_2$ (0.50 ± 0.5) at 10 K which reflect the similar values for k_{on} for the two species. Structurally, similar proximal barriers to oxygen binding are supported by similar metal−heme displacements in the deoxy, oxy, and low temperature photoproduct states of CoMb and FeMb.

The unique values for k_{off} in $CoMbO_2$ and $FeMbO_2$ seem to arise from different distal barriers to oxygen release. X-ray edge positions of deoxy and oxy CoMb and FeMb indicate a similar and substantial degree of electron transfer from the metal to the ligand upon oxygenation. Metal−oxygen and dioxygen stretching frequencies for $CoMbO_2$ and $FeMbO_2$ demonstrate that the distribution of that electron density differs in $CoMbO_2$ versus $FeMbO_2$. Weaker Co−O versus Fe−O bonds have been identified in cobaltous and ferrous myoglobin and model compounds by RR spectroscopy (Tsubaki & Yu, 1981). We have determined that ν(O−O) for $CoMbO_2$ (~1138 cm^{-1}) is higher than $FeMbO_2$ (~1131 cm^{-1}) and the dioxygen stretching frequency in $CoMbO_2$ is closer to that of non-hydrogen-bonded models. Thus, the differences between the electronic configurations of the Co−O−O and Fe−O−O moieties and their interactions with the distal pocket are supportive of different distal barriers to oxygen dissociation in myoglobin.

ACKNOWLEDGMENT

We gratefully thank Dr. H. Caroline Lee for the cobalt myoglobin samples and a critical review of the manuscript, Dr. Jack Peisach for his helpful comments, and Dr. Yang Hai and Michael Sullivan for technical assistance. The construction and operation of beamline X9B at the NSLS is supported by a grant from the NIH (RR-01633). The NSLS is supported by the Department of Energy, Division of Material Sciences and Division of Chemical Science.

REFERENCES

Ahmed, A. M., Campbell, B. F., Caruso, D., Chance, M. R., Chavez, M. D., Courtney, S. H., Friedman, J. M., Iben, I. E. T., Ondrias, M. R., & Yang, M. (1991) *Chem. Phys. 158*, 329.

Antonini, E., & Brunori, M. (1971) *Hemoglobin and Myoglobin in Their Reactions with Ligands*,North-Holland, New York.

Austin, R. H., Beeson, K., Eisenstein, L., Frauenfelder, H., & Gunsalus, I. C. (1975) *Biochemistry 14*, 5355.

Bajdor, K., Kincaid, J. R., & Nakamoto, K. (1984) *J. Am. Chem. Soc. 106*, 7741.

Barlow, C. H., Maxwell, J. C., Wallace, W. J., & Caughey, W. S. (1973) *Biochem. Biophys. Res. Commun. 55*, 91.

Belli, M., Scafati, A., Bianconi, A., Mobilio, S., Palladino, L., Reale, A., & Burattini, E. (1980) *Solid State Commun. 35*, 355.

Bertini, I., Gray, H. B., Lippard, S. J., & Valentine, J. S. (1994) *Bioinorganic Chemistry*, University Science Books, Mill Valley, CA.

Bianconi, A., Congiu-Castellano, A., Dell'Ariccia, M., Giovannelli, A., Durham, P. J., Burattini, E., & Marteri, M. (1984) *FEBS Lett. 178*, 165.

Bruha, A., & Kincaid, J. R. (1988) *J. Am. Chem. Soc. 110*, 6006.
Brunori, M., Antonini, E., Phelps, C., & Amiconi, G. (1969) *J. Mol. Biol. 44*, 563.
Carver, T. E., Rohlfs, R. J., Olson, J. S., Gibson, Q. H., Blackmore, R. S., Springer, B. A., & Sligar, S. G. (1990) *J. Biol. Chem. 265*, 20007.
Chance, B., Powers, L., Ching, Y., Poulos, T., Schonbaum, G. R., Yamazaki, I., & Paul, K. G. (1984) *Arch. Biochem. Biophys. 235*, 596.
Chance, M. R. (1986) *The Proximal Ligand in Enzyme Function*, Ph.D. Dissertation, University of Pennsylvania.
Chance, M. R., Parkhurst, L. J., Powers, L. S., & Chance, B. (1986) *J. Biol. Chem. 261*, 5689.
Chance, M. R., Courtney, S. H., Chavez, M. D., Ondrias, M. R., & Friedman, J. M. (1990) *Biochemistry 29*, 5537.
Chien, J. C. W., & Dickinson, L. C. (1972) *Proc. Natl. Acad. Sci. U.S.A. 69*, 2783.
Collman, J. P., Gagne, R. R., Reed, C. A., Halbert, T. R., Lang, G., & Robinson, W. T. (1975) *J. Am. Chem. Soc. 97*, 1427.
Collman, J. P., Brauman, J. I., Halbert, T. R., & Suslick, K. S. (1976) *Proc. Natl. Acad. Sci. U.S.A. 73*, 3333.
Collman, J. P., Brauman, J. I., Doxsee, K. M., Halbert, T. R., & Suslick, K. S. (1978) *Proc. Natl. Acad. Sci. U.S.A. 75*, 564.
Cramer, S. P., Tench, O., Yocum, M., & George, G. N. (1988) *Nucl. Instrum. Methods A266*, 586.
Doster, W., Beece, D., Bowne, S. F., Dilorio, E. E., Eisenstein, L., Frauenfelder, H., Reinisch, L., Shyamsunder, E., Winterhalter, K. H., & Yue, K. T. (1982) *Biochemistry 21*, 4831.
Fabry, T. L., Simo, C., & Javaherian, K. (1968) *Biochim. Biophys. Acta 160*, 118.
Fermi, G., Perutz, M. F., Dickinson, L. C., & Chien, J. C. W. (1982) *J. Mol. Biol. 155*, 495.
Friedman, J. M., Rousseau, D. L., Ondrias, M. R., & Stepnoski, R. A. (1982) *Science 218*, 1244.
Friedman, J. M., Scott, T. W., Fisanick, G. J., Simon, S. R., Findsen, E. W., Ondrias, M. R., & MacDonald, V. W. (1985) *Science 229*, 187.
Gibson, Q. H., Regan, R., Elbers, R., Olson, J. S., & Carver, T. E. (1992) *J. Biol. Chem. 267*, 22022.
Hoffman, B. M., & Petering, D. H. (1970) *Proc. Natl. Acad. Sci. U.S.A. 67*, 637.
Hori, H., Ikeda-Saito, M., Leigh, J. S. J., & Yonetani, T. (1982) *Biochemistry 21*, 1431.
Hu, S., Vogel, K. M., & Spiro, T. G. (1994) *J. Am. Chem. Soc. 116*, 11187.
Ikeda-Saito, M., Iizuka, T., Yamamato, H., Kayne, F. J., & Yonetani, T. (1977) *J. Biol. Chem. 252*, 4882.
Ikeda-Saito, M., Lutz, R. S., Shelley, D. A., McKelvey, E. J., Mattera, R., & Hori, H. (1991) *J. Biol. Chem. 266*, 23641.
Kincaid, J. R., Proniewicz, L. M., Bajdor, K., Bruha, A., & Nakamoto, K. (1985) *J. Am. Chem. Soc. 107*, 6775.
Kuriyan, J., Wilz, S., Karplus, M., & Petsko, G. A. (1986) *J. Mol. Biol. 192*, 133.
Lee, H. C., Ikeda-Saito, M., Yonetani, T., Maggliozo, R. S., & Peisach, J. (1992) *Biochemistry 31*, 7274.
Lee, H. C., Peisach, J., Dou, Y., & Ikeda-Saito, M. (1994) *Biochemistry 33*, 7609.
Li, X. Y., & Spiro, T. G. (1988) *J. Am. Chem. Soc. 110*, 6024.
Maxwell, J. C., & Caughey, W. S. (1974) *Biochem. Biophys. Res. Commun. 60*, 1309.
Maxwell, J. C., Volpe, J. A., Barlow, C. H., & Caughey, W. S. (1974) *Biochem. Biophys. Res. Commun. 58*, 166.
Miller, L. M., & Chance, M. R. (1994) *J. Am. Chem. Soc. 116*, 9662.
O'Hagen, J. E. (1961) *Haematin Enzymes 173*, Pergamon Press, London.
Padlan, E. A., Eaton, W. A., & Yonetani, T. (1975) *J. Biol. Chem. 250*, 7069.
Petrich, J., Poyart, C., & Martin, J. (1988) *Biochemistry 27*, 4049.
Petsko, G. A., Rose, D., Tsernoglou, D., Ikeda-Saito, M., & Yonetani, T. (1978) *Frontiers of Biological Energetics* (Dutton, P. L., Leigh, J. S., Jr. & Scarpa, A., Eds.) 1010, Academic Press, New York.
Phillips, S. E. V. (1980) *J. Mol. Biol. 142*, 531.
Phillips, S. E. V. (1981) Brookhaven Protein Data Bank, file name 1MBD.
Potter, W. T., Tucker, M. P., Houtchens, R. A., & Caughey, W. S. (1987) *Biochemistry 26*, 4699.
Powers, L., Chance, B., Chance, M. R., Campbell, B., Friedman, J., Khalid, S., Kumar, C., Naqui, A., Reddy, K. S., & Zhou, Y. (1987) *Biochemistry 26*, 4785.
Proniewicz, L. M., & Kincaid, J. R. (1990) *J. Am. Chem. Soc. 112*, 675.
Proniewicz, L. M., Bruha, A., Nakamoto, K., Kyuno, E., & Kincaid, J. R. (1989) *J. Am. Chem. Soc. 111*, 7050.
Quillin, M. L., Arduini, R. M., Olson, J. S., & Phillips, G. N. (1993) *J. Mol. Biol. 234*, 140.
Quillin, M. L., Li, T., Olson, J. S., Phillips, G. N., Dou, Y., Ikeda-Saito, M., Regan, R., Carlson, M., Gibson, Q. H., Li, H., et al. (1995) *J. Mol. Biol. 245*, 416.
Ray, G. B., Li, X. Y., Ibers, J. A., Sessler, J. L., & Spiro, T. G. (1994) *J. Am. Chem. Soc. 116*, 162.
Reed, C. A., & Cheung, S. K. (1977) *Proc. Natl. Acad. Sci. U.S.A. 74*, 1780.
Rohlfs, R. J., Mathews, A. J., Carver, T. E., Olson, J. S., Springer, B. A., Egeberg, K. D., & Sligar, S. G. (1990) *J. Biol. Chem. 265*, 3168.
Scheidt, W. R., & Hoard, J. L. (1973) *J. Am. Chem. Soc. 95*, 8281.
Scheuring, E. M., Sagi, I., & Chance, M. R. (1994) *Biochemistry 33*, 6310.
Schlichting, I., Berendsen, J., Phillips, G. N., & Sweet, R. M. (1994) *Nature 371*, 808.
Scott, T. W., Friedman, J. M., & MacDonald, V. W. (1985) *J. Am. Chem. Soc. 107*, 3702.
Shiro, Y., Makino, R., Sato, F., Oyanagi, H., Matsushita, T., Ishimura, Y., & Iizuka, T. (1991) *Biochim. Biophys. Acta 1115*, 101.
Smulevich, G., Evangelista-Kirkup, R., English, A., & Spiro, T. G. (1986) *Biochemistry 25*, 4426.
Spartalian, K., Lang, G., & Yonetani, T. (1976) *Biochim. Biophys. Acta 428*, 281.
Srajer, V., Reinisch, L., & Champion, P. M. (1988) *J. Am. Chem. Soc. 110*, 6656.
Tsubaki, M., & Yu, N. T. (1981) *Proc. Natl. Acad. Sci. U.S.A. 78*, 3581.
Tsubaki, M., Srivastava, R. B., & Yu, N. T. (1982) *Biochemistry 21*, 1132.
Uno, T., Nishimura, T., Tsuboi, M., Makino, R., Iizuka, T., & Ishimura, Y. (1987) *J. Biol. Chem. 262*, 4549.
Walters, M. A., Spiro, T. G., Suslick, K. S., & Collman, J. P. (1980) *J. Am. Chem. Soc. 102*, 6857.
Wayland, B. B., Minkiewicz, J. V., & Abd-Elmageed, M. E. (1974) *J. Am. Chem. Soc. 96*, 2795.
Wirt, M. D., Sagi, I., Chen, E., Frisbie, S. M., Lee, R., & Chance, M. R. (1991) *J. Am. Chem. Soc. 113*, 5299.
Wirt, M. D., Kumar, M., Ragsdale, S. W., & Chance, M. R. (1993) *J. Am. Chem. Soc. 115*, 2146.
Wong, J., Lytle, F. W., Messmer, R. P., & Maylotte, D. H. (1984) *Phys. Rev. B. 30*, 5596.
Yamamoto, H., Kayne, F. J., & Yonetani, T. (1974) *J. Biol. Chem. 249*, 691.
Yonetani, T., Drott, H. R., Leigh, J. S. J., Reed, G. H., Waterman, M. R., & Asakura, T. (1970) *J. Biol. Chem. 245*, 2998.
Yonetani, T., Yamamato, H., & Iizuka, T. (1974a) *J. Biol. Chem. 249*, 2168.
Yonetani, T., Yamamato, H., & Woodrow, G. V., III (1974b) *J. Biol. Chem. 249*, 682.

BI950448Q